Available online at www.sciencedirect.com
SCIENCE DIRECT®
Journal of Solid State Chemistry 172 (2003) 438–445
JOURNAL OF SOLID STATE CHEMISTRY
http://elsevier.com/locate/jssc

Magnetic and calorimetric studies on rare-earth iron borates $LnFe_3(BO_3)_4$ (Ln = Y, La–Nd, Sm–Ho)

Yukio Hinatsu,[a,*] Yoshihiro Doi,[a] Kentaro Ito,[a] Makoto Wakeshima,[a] and Abdolali Alemi[b,1]

[a] *Division of Chemistry, Graduate School of Science, Hokkaido University, Sapporo 060-0810, Japan*
[b] *Inorganic Synthesis Laboratory, Faculty of Chemistry, Tabriz University, Tabriz, Iran*

Received 17 September 2002; received in revised form 25 November 2002; accepted 11 December 2002

Abstract

A series of rare-earth iron borates having general formula $LnFe_3(BO_3)_4$ (Ln = Y, La–Nd, Sm–Ho) were prepared and their magnetic properties have been investigated by the magnetic susceptibility, specific heat, and ^{57}Fe Mössbauer spectrum measurements. These borates show antiferromagnetic transitions at low temperatures and their magnetic transition temperatures increase with decreasing Ln^{3+} ionic radius from 22 K for $LaFe_3(BO_3)_4$ to 40 K for $TbFe_3(BO_3)_4$. In addition, X-ray diffraction, specific heat, and differential thermal analysis (DTA) measurements indicate that the phase transition occurs for the $LnFe_3(BO_3)_4$ compounds with Ln = Eu–Ho, Y, and its transition temperature increases remarkably with decreasing Ln^{3+} ionic radius from 88 K for Ln = Eu to 445 K for Ln = Y.

Keywords: Magnetic properties; Specific heat; Rare-earth; Borate; Ion; ^{57}Fe Mössbauer Spectroscopy

1. Introduction

Borate crystals with the structure of the naturally occurring mineral huntite $CaMg_3(CO_3)_4$ are widely known as polyfunctional materials having device potential due to their good thermal and chemical stabilities. The general formula of the huntite borates is $LnM_3(BO_3)_4$, where Ln designates a rare-earth element and M is a trivalent Al, Ga, Cr, Fe, or Sc [1,2]. Among them, rare–earth aluminium borates [$LnAl_3(BO_3)_4$] have attracted considerable attention for their luminescence properties and possible application as single crystal minilasers [3].

We have been studying the structural chemistry and magnetic properties of mixed-metal oxides containing both rare-earth and transition elements. Special interest has been paid on the ordered perovskite-type oxides A_2LnMO_6 (A = Sr, Ba; Ln = lanthanide element, M = 4d or 5d transition element) in which the Ln and M ions regularly order. These compounds show an antiferromagnetic transition at low temperatures and weak ferromagnetic moments associated with the antiferromagnetism are also found [4–10]. The results of the magnetic susceptibility, specific heat, and neutron diffraction measurements show that their peculiar magnetic behavior is due to the properties of both the lanthanide (unpaired 4f electrons) and the transition elements (unpaired d electrons).

In this study, our attention has been focused on the rare–earth iron borates $LnFe_3(BO_3)_4$ in which both the rare earth and the iron should contribute to their magnetic properties. Crystal structures of these borates are rhombohedral and belong to the space group $R32$ [11]. The crystal structure of huntite was analyzed by Graf and Bradly [12]. Fig. 1 shows the schematic diagram of the huntite structure. The oxygen framework involves three types of non-equivalent cation sites. The Ln^{3+} ion is surrounded by a trigonal prism of six oxygens, each belonging to a different borate group and not shared by neighboring Ln^{3+} ions. Fe^{3+} ions are octahedrally coordinated by six oxygen atoms. The B^{3+} ions are in the centers of triangles formed by three adjacent oxygen atoms. The structure can be seen as a

*Corresponding author. Fax: +81-11-706-4294.
E-mail address: hinatsu@sci.hokudai.ac.jp (Y. Hinatsu).
[1] Present address: Division of Chemistry, Graduate School of Science, Hokkaido University, Sapporo 060-0810, Japan.

0022-4596/03/$ - see front matter © 2003 Elsevier Science (USA). All rights reserved.
doi:10.1016/S0022-4596(03)00028-8

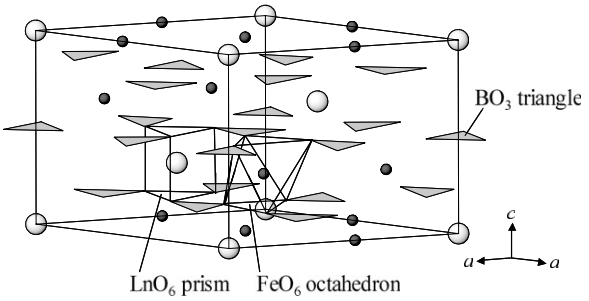

Fig. 1. Schematic crystal structure of LnFe$_3$(BO$_3$)$_4$ compounds.

succession of layers perpendicular to the c-axis, alternating BO_3 and Ln+Fe planes. This unique crystal structure may cause interesting magnetic phenomena at low temperatures. Since both the rare earth and the iron should contribute to the magnetic properties of LnFe$_3$(BO$_3$)$_4$, they may be complicated. Here, we have prepared a series of LnFe$_3$(BO$_3$)$_4$ and performed measurements of their magnetic susceptibility, specific heat, differential thermal analysis (DTA), and ^{57}Fe Mössbauer spectrum. Through these measurements, the magnetic properties of LnFe$_3$(BO$_3$)$_4$ will be elucidated.

2. Experimental

2.1. Sample preparation

A mixture with the molar ratio Ln_2O_3: Fe_2O_3: H_3BO_3 = 1:3:8 (with a 10% excess of H_3BO_3) was prepared in an agate mortar. The samples were pressed into pellets, and the pellets were heated slowly to 800°C and kept at this temperature for 12 h to achieve dehydration. The samples were then ground, pressed again, and sealed in gold tubing to avoid the evaporation of B_2O_3. The final reaction temperature was 980°C. After 3 days at 980°C, the furnace was switched off and the samples were allowed to cool. For the obtained products, X-ray diffraction measurements were performed in order to check whether the desired compounds were prepared. When impurities such as starting materials Ln_2O_3 or Fe_2O_3 were found in the products, an additional H_3BO_3 was mixed with the products. They were well ground, re-pressed, and heated to 800°C. Then, the mixtures were reground, re-pressed, and sealed again in gold tubing. The final reaction temperature was 980°C. In addition to a series of LnFe$_3$(BO$_3$)$_4$ compounds, a GdGa$_3$(BO$_3$)$_4$ compound was also prepared by heating an appropriate amount of Gd_2O_3, Ga_2O_3, and H_3BO_3. This compound is needed to estimate the magnetic entropy due to the magnetic ordering of Fe^{3+} ions, as will be described later. The heating procedures were the same as in the case of LnFe$_3$(BO$_3$)$_4$. The progress of the reactions was monitored by powder X-ray diffraction measurements.

2.2. X-ray diffraction analysis

Powder X-ray diffraction measurements were carried out in the region of $10° \leqslant 2\theta \leqslant 120°$ using Cu$K\alpha$ radiation on a Rigaku MultiFlex diffractometer equipped with a curved graphite monochromator.

2.3. Magnetic susceptibility measurements

The temperature dependence of the magnetic susceptibility was measured in an applied field of 0.1 T over the temperature range of $1.8\,K \leqslant T \leqslant 300\,K$, using a SQUID magnetometer (Quantum Design, MPMS5S). The susceptibility measurements were performed using either zero-field cooling (ZFC) or field cooling (FC) conditions. The former was measured upon heating the sample to 300 K under the applied magnetic field of 0.1 T after ZFC to 1.8 K. The latter was measured upon cooling the sample from 300 to 1.8 K at 0.1 T. For some samples, the experimental temperature range was extended up to 400 K.

2.4. Specific heat and DTA measurements

Specific heat measurements were performed using a relaxation technique by a commercial heat capacity measuring system (Quantum Design, PPMS) in the temperature range 1.8–400 K. The sintered sample in the form of a pellet was mounted on a thin alumina plate with Apiezon for better thermal contact. The DTA measurements were carried out in the temperature range of $300\,K \leqslant T \leqslant 600\,K$ using TG-DTA2000S (MAC Science Co., Ltd).

2.5. ^{57}Fe Mössbauer spectrum measurements

The ^{57}Fe Mössbauer spectrum for EuFe$_3$(BO$_3$)$_4$ was measured with a conventional transmissional Mössbauer spectrometer VT-6000 (Laboratory Equipment Co., Japan) in the constant acceleration mode. Absorbers were prepared from finely ground EuFe$_3$(BO$_3$)$_4$ which was weighed to give optimum signal to noise and mixed with carbon in order to randomize the orientations of the microcrystals. A source of up to 100 mCi of ^{57}Co in Rh was used and the spectrometer was calibrated using α-iron at room temperature. The sample lapped in an aluminum foil was cooled down to 15 K by using a variable temperature cryostat system Cryomini (Iwatani Industrial Gases Co., Japan).

3. Results and discussion

3.1. Crystal structure

X-ray diffraction measurements show that rare–earth iron borates $LnFe_3(BO_3)_4$ were obtained as single phases for Ln = Y, La–Nd, and Sm–Ho. Fig. 2 shows the observed and calculated diffraction patterns for $TbFe_3(BO_3)_4$ as an example, and Table 1 lists its lattice parameters and atomic positions refined by the Rietveld analysis. The crystals have a rhombohedral lattice with three formula in the unit cell. The space group is $R32$. The crystal structure is shown in Fig. 1. Fig. 3 shows the lattice parameters for $LnFe_3(BO_3)_4$ as a function of the Ln^{3+} ionic radius. Both the a and c parameters increase with the Ln^{3+} ionic radius, as expected.

3.2. Magnetic properties

Through measurements of the magnetic susceptibility, specific heat, and DTA on these $LnFe_3(BO_3)_4$ compounds, we have found one or two anomalies for any compound in their temperature dependence and their results are listed in Table 2. No divergence between the ZFC and FC susceptibilities have been found for any compound throughout the whole experimental temperature range.

3.2.1. $LaFe_3(BO_3)_4$

The temperature dependence of the magnetic susceptibility and specific heat for $LaFe_3(BO_3)_4$ is depicted in Fig. 4. This compound shows a typical antiferromagnetic behavior at low temperatures. The magnetic susceptibilities have a maximum at 26 K, and decrease rapidly with temperature at 22 K. At nearly the same temperature (23 K), a λ-type specific heat anomaly has been observed. These are due to the magnetic interactions between Fe^{3+} ions which are the only paramagnetic ions in the $LaFe_3(BO_3)_4$. The temperature dependence of the reciprocal magnetic susceptibility shows a linear relationship above the magnetic transition temperature. By applying the Curie–Weiss law, the effective magnetic moment per mole of this compound and the Weiss constant are determined to be 10.5 μ_B and -124 K, respectively. Considering the magnetic moment of the Fe^{3+} ion to be $\mu_{eff} = 5.916\,\mu_B$ ($= 2\sqrt{S(S+1)}$, where S is a total spin quantum number and $S = 5/2$ for a Fe^{3+} ion), the effective magnetic moment of this compound is calculated to be 10.2 μ_B ($= \sqrt{3} \times \mu_{eff}$), which is in good agreement with the experimental result. The negative Weiss constant also indicates that the magnetic exchange interaction found in this compound is antiferromagnetic.

3.2.2. $LnFe_3(BO_3)_4$ (Ln=Ce, Pr, Nd, Sm)

The temperature dependence of the magnetic susceptibility and specific heat for $LnFe_3(BO_3)_4$ (Ln = Ce, Pr, Nd. Sm) is quite similar to that for $LaFe_3(BO_3)_4$. Both the magnetic susceptibility and specific heat show the existence of an antiferromagnetic transition at 28—33 K. Fig. 5 shows the antiferromagnetic transition temperature (T_N) against the Ln^{3+} ionic radius,

Table 1
Atomic positional parameters for $TbFe_3(BO_3)_4$ at room temperature

Atom	Site	x	y	z
Tb	3a	0	0	0
Fe	9d	0.5499(7)	0	0
B(1)	3b	0	0	1/2
B(2)	9e	0.626(5)	0	1/2
O(1)	9e	−0.153(3)	0	1/2
O(2)	9e	−0.434(3)	0	1/2
O(3)	18f	0.448(2)	0.139(2)	0.517(3)

Note: space group: $R32$ (No. 155), $z = 3$; $a = 9.5466(2)$ Å, $c = 7.5704(1)$ Å, $V = 597.51(2)$ Å^3, $B = 0.3$ Å^2 (fixed), $R_{wp} = 16.35\%$, $R_I = 5.46\%$, $R_F = 3.47\%$, $R_e = 11.60\%$.

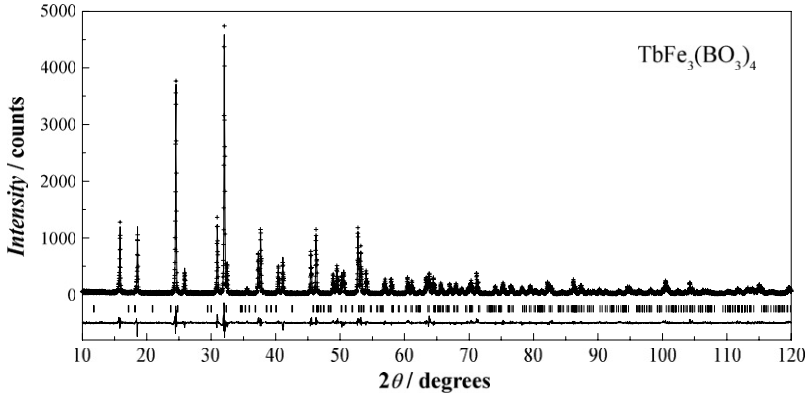

Fig. 2. Powder X-ray diffraction profile for $TbFe_3(BO_3)_4$ at room temperature. The calculated and observed profiles are shown on the top solid line and cross markers, respectively. The vertical marks in the middle show positions calculated for Bragg reflections. The lower trace is a plot of the difference between calculated and observed intensities.

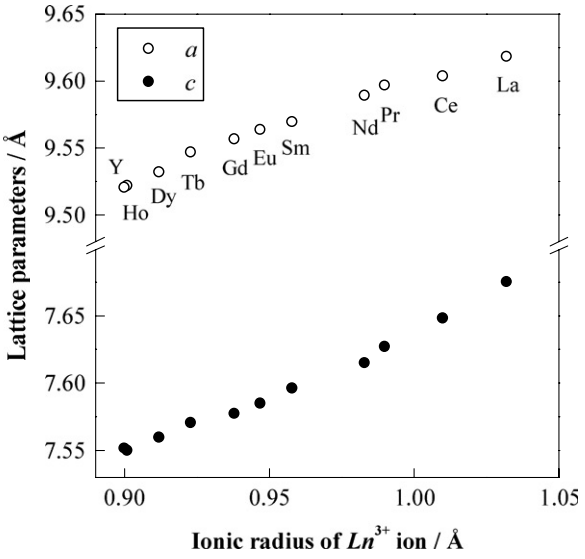

Fig. 3. Lattice parameters vs. Ln^{3+} ionic radius for $LnFe_3(BO_3)_4$.

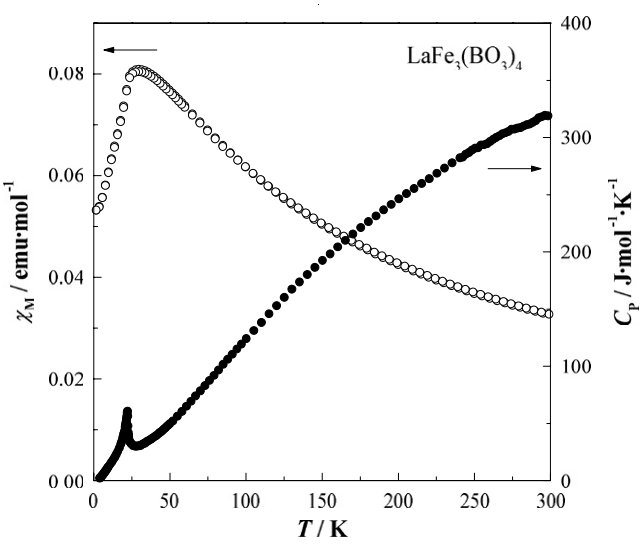

Fig. 4. Temperature dependence of the magnetic susceptibility and specific heat for $LaFe_3(BO_3)_4$.

Table 2
Temperatures at which anomalies have been observed by the magnetic susceptibility, specific heat, and DTA measurements for $LnFe_3(BO_3)_4$

Ln	Magnetic susceptibility	Specific heat	DTA
La	22	23	
Ce	28	28	
Pr	30	31	
Nd	30	31	
Sm	32	33	
Eu	32	34 88	
Gd	36	37 174	
Tb	40	40 241	
Dy	30	39 340	
Ho	(6)	39	427
Y	38	38	445

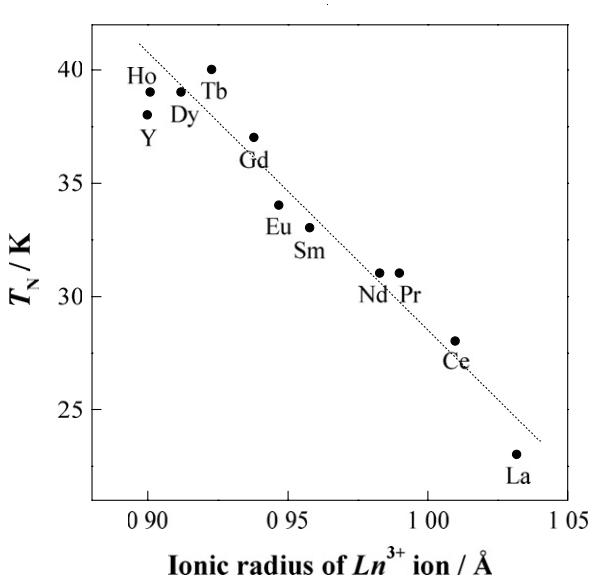

Fig. 5. Antiferromagnetic transition temperature vs. Ln^{3+} ionic radius.

indicating that the transition temperature increases with decreasing size of the Ln^{3+} ion (therefore, the decrease of lattice parameter). This result is consistent with the general rule that the magnetic interaction between Fe^{3+} ions increases with decreasing their distance.

3.2.3. $EuFe_3(BO_3)_4$

Fig. 6 shows the temperature dependence of the magnetic susceptibility and specific heat for $EuFe_3(BO_3)_4$. In addition to the antiferromagnetic transition at 34 K, another anomaly has been found in the specific heat vs. temperature curve at 88 K. As will be described later, this second anomaly in the specific heat has been observed for any $LnFe_3(BO_3)_4$ compound with Ln = Eu, Gd–Ho, and its temperature increases remarkably with decreasing Ln^{3+} ionic radius (see Table 2). The origin of this anomaly is due to the phase transition, which is elucidated by the high-temperature X-ray diffraction measurements for $DyFe_3(BO_3)_4$ and by the DTA measurements for $HoFe_3(BO_3)_4$ and $YFe_3(BO_3)_4$, as will be described in later section.

3.2.4. $LnFe_3(BO_3)_4$ (Ln=Gd–Dy)

The temperature dependence of the magnetic susceptibility and specific heat for $LnFe_3(BO_3)_4$ (Ln = Gd–Dy) is quite similar to that for $EuFe_3(BO_3)_4$, i.e., two anomalies have been observed in the specific heat vs. temperature curve, and the lower one is due to the antiferromagnetic ordering of Fe^{3+} ions and the higher

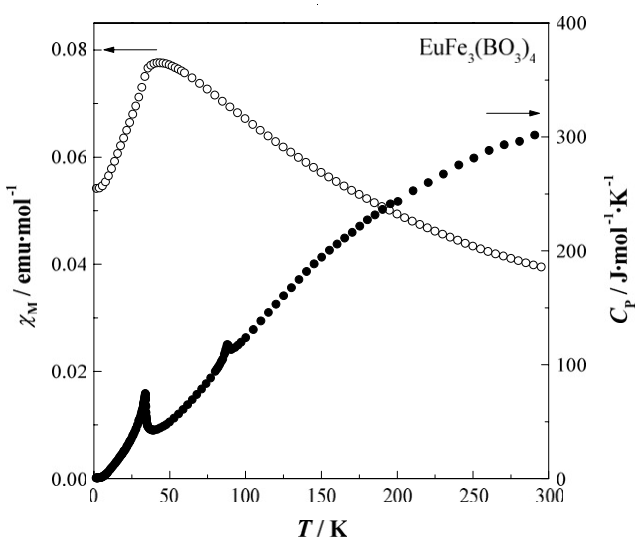

Fig. 6. Temperature dependence of the magnetic susceptibility and specific heat for $EuFe_3(BO_3)_4$.

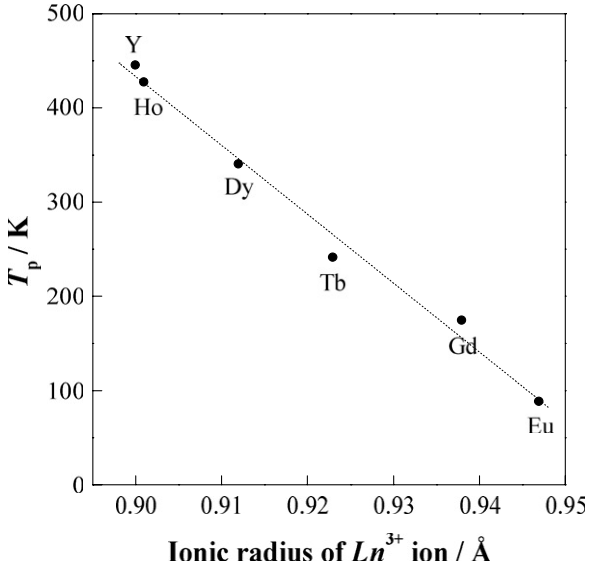

Fig. 7. The temperature at which the specific heat anomaly or DTA peak appears vs. Ln^{3+} ionic radius.

one is considered to be ascribable to the phase transition. In Fig. 7, the temperatures at which the latter anomalies have been observed (T_P) are plotted against the Ln^{3+} ionic radius. They increase almost linearly with decreasing Ln^{3+} size.

Specific heat measurements for $DyFe_3(BO_3)_4$ show that in addition to the specific heat anomaly at 39 K (which is due to the antiferromagnetic ordering of Fe^{3+} ions), another specific heat anomaly has been observed at 340 K (see Table 2). So, we have performed its X-ray diffraction measurements in the temperature range 300–420 K. Fig. 8 shows the temperature dependence of the lattice parameters a and c. A significant change has been observed in the lattice parameter a at 340 K,

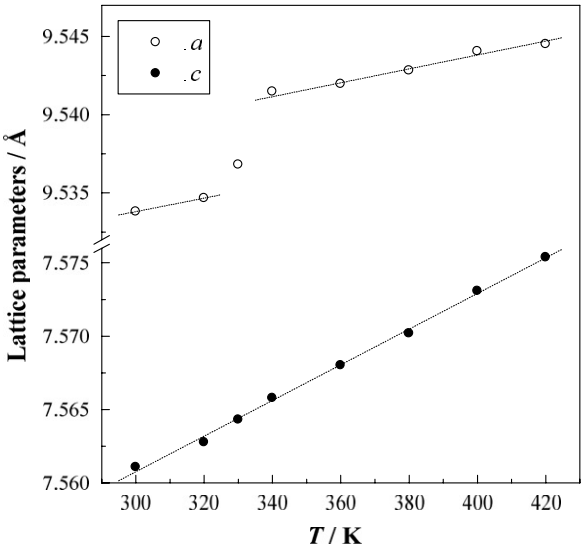

Fig. 8. Temperature dependence of the lattice parameters for $DyFe_3(BO_3)_4$.

indicating that there occurs a first-order transition at this temperature in this $DyFe_3(BO_3)_4$ compound. Unfortunately, we could not elucidate the crystal structure in the high temperature phase.

Although most of the $LnAl_3(BO_3)_4$ (Ln = Y, La–Lu) compounds belong to the huntite type of structure with $R32$ space group, Pr, Nd, Sm, Eu, and Gd borates also have high-temperature monoclinic modifications with the phase transition temperatures of 1080°C, 880–900°C, 1130–1150°C, 1130–1150°C, and 1040–1050°C, respectively [13], but no systematic change in the phase transition temperature vs. the rare-earth size was reported. On the other hand, it has been reported that ternary lithium rare earth oxides $LiLnO_2$ (Ln = Dy, Ho, Y, Er) transform from the monoclinic β-type to the tetragonal α-type structures at 475, 360, 325, and 200 K, respectively [14]. The transition temperature of $LiLnO_2$ increases linearly with the Ln^{3+} ionic radius, which is contrastive to the present result (Fig. 7).

3.2.5. $HoFe_3(BO_3)_4$

Fig. 9 shows the temperature dependence of the magnetic susceptibility and specific heat for $HoFe_3(BO_3)_4$. Although a clear λ-type specific heat anomaly has been observed at 39 K, the magnetic susceptibility increases with decreasing temperature and then turns to decrease when the temperature is decreased through 6 K. The result that the susceptibility does not show any magnetic anomaly at the same temperature at which the λ-type specific heat anomaly appears is due to the large effective magnetic moment of Ho^{3+} ion. That is, the paramagnetic behavior of Ho^{3+} ion obscures the antiferromagnetic interaction between the Fe^{3+} ions in the magnetic susceptibility vs. temperature curve. The second specific heat anomaly was not observed in the

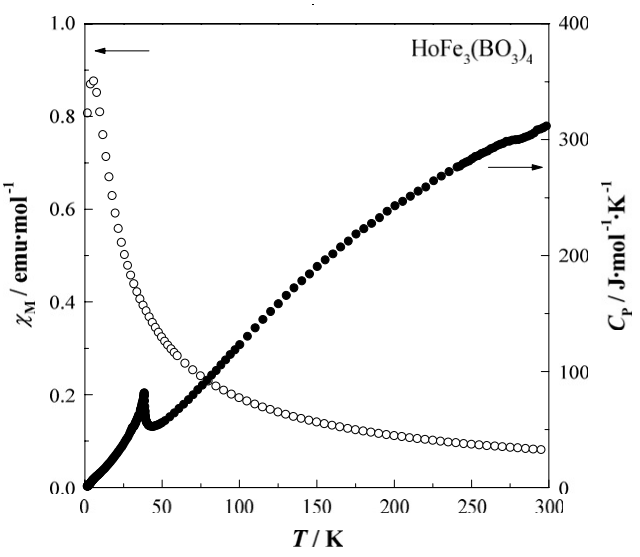

Fig. 9. Temperature dependence of the magnetic susceptibility and specific heat for $HoFe_3(BO_3)_4$.

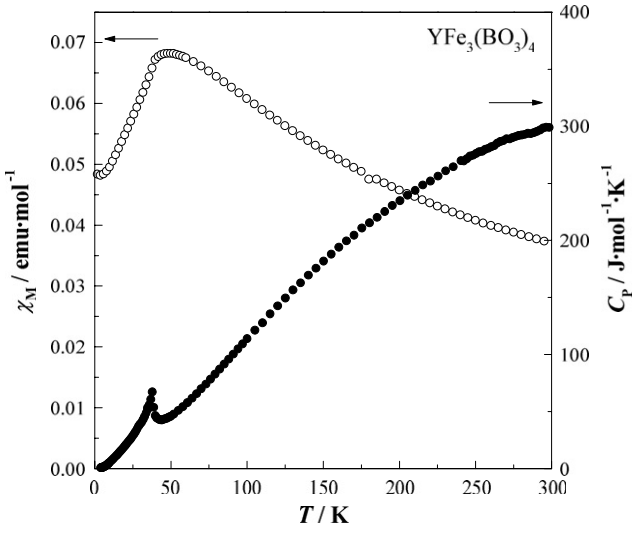

Fig. 10. Temperature dependence of the magnetic susceptibility and specific heat for $YFe_3(BO_3)_4$.

experimental temperature range (1.8–400 K). If we assume that the linear relationship holds between the temperature at which the second specific heat anomaly appears (T_P) and the Ln^{3+} ionic radius (see Fig. 7), the T_P temperature for the $HoFe_3(BO_3)_4$ should be ~425 K which is beyond our experimental temperature range. So, we carried out DTA measurements in the temperature range between 300 and 600 K. An endothermal peak has been observed at 427 K in the DTA curve during heating, as expected (see Table 2).

3.2.6. $YFe_3(BO_3)_4$

The temperature dependence of the magnetic susceptibility and specific heat for $YFe_3(BO_3)_4$ is shown in Fig. 10. It is quite similar to the temperature dependence for $LaFe_3(BO_3)_4$. The magnetic transition temperature observed for $YFe_3(BO_3)_4$ is 38 K, which is much higher than that for $LaFe_3(BO_3)_4$. Fig. 11 shows the results of the DTA measurements for $YFe_3(BO_3)_4$, indicating the exothermal peak at 445 K during cooling. This result is in an agreement with the linear relationship between the T_P temperature and the Ln^{3+} ionic radius (see Fig. 7).

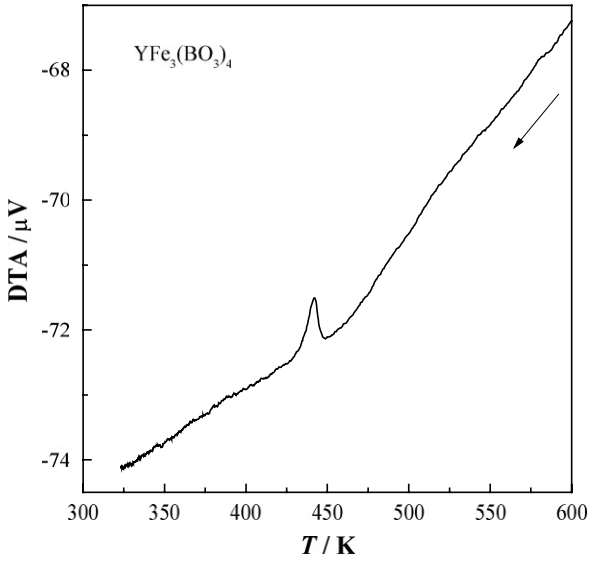

Fig. 11. DTA curve during cooling for $YFe_3(BO_3)_4$.

Table 3
Experimental effective magnetic moments (μ_{exp}), calculated moments (μ_{calc}), and Weiss constants (θ) for $LnFe_3(BO_3)_4$

Ln	μ_{exp} (μ_B)	μ_{calc} (μ_B)	θ (K)
La	10.5	10.2	−124
Ce	11.6	10.6	−147
Pr	10.9	10.9	−111
Nd	11.2	10.9	−115
Sm	10.5	10.3	−154
Eu	11.3	10.2	−170
Gd	12.9	13.0	−51
Tb	14.1	14.1	−55
Dy	12.7	14.8	−145
Ho	15.2	14.7	−63
Y	12.8	10.2	−248

3.3. Effective magnetic moments

Above the magnetic transition temperatures, magnetic susceptibilities of these $LnFe_3(BO_3)_4$ compounds follow the Curie–Weiss law. Table 3 summarizes the effective magnetic moments and Weiss constants for $LnFe_3(BO_3)_4$. Except for $LaFe_3(BO_3)_4$ and $YFe_3(BO_3)_4$, there are two kinds of magnetic ions, i.e., Ln^{3+} and Fe^{3+} ions in each of the $LnFe_3(BO_3)_4$ compounds. The effective magnetic moments of $LnFe_3(BO_3)_4$ are calculated from the equation

$\mu_{calc}^2 = \mu_{eff}(Ln^{3+})^2 + 3\mu_{eff}(Fe^{3+})^2$. They agree with the moments experimentally obtained for $LnFe_3(BO_3)_4$ (μ_{exp}). The negative Weiss constants for all of these compounds indicate that the predominant magnetic interactions are antiferromagnetic.

3.4. Specific heat analysis

Fig. 10 clearly shows the existence of the second order phase transition, i.e., the magnetic transition at 38 K in the $YFe_3(BO_3)_4$. Since the Fe^{3+} ions are only paramagnetic ions, the transition observed at 38 K is surely ascribable to the antiferromagnetic ordering of Fe^{3+} ions.

To estimate the magnetic entropy change for the magnetic ordering of Fe^{3+} ions, we evaluated it by using the results of the specific heat measurements on $GdGa_3(BO_3)_4$ which is isomorphous with $LnFe_3(BO_3)_4$. Fig. 12 shows the temperature dependence of the reciprocal magnetic susceptibility and the specific heat for $GdGa_3(BO_3)_4$. It shows that $GdGa_3(BO_3)_4$ is paramagnetic down to 1.8 K. The magnetic entropy change due to the magnetic ordering of Fe^{3+} ions at 38 K in the $YFe_3(BO_3)_4$ was determined by assuming that the electronic and lattice contribution to the specific heat of the $YFe_3(BO_3)_4$ was equal to the specific heat of $GdGa_3(BO_3)_4$ (see the inset of Fig. 13(a)). In the temperature region below 6 K, we assumed that the lattice contribution to the specific heat of $GdGa_3(BO_3)_4$ is proportional to the third power of temperature (see a dotted line in the inset of Fig. 12). Then, the magnetic specific heat (C_{mag}) for $YFe_3(BO_3)_4$ is obtained by subtracting the specific heat of $GdFe_3(BO_3)_4$ from that

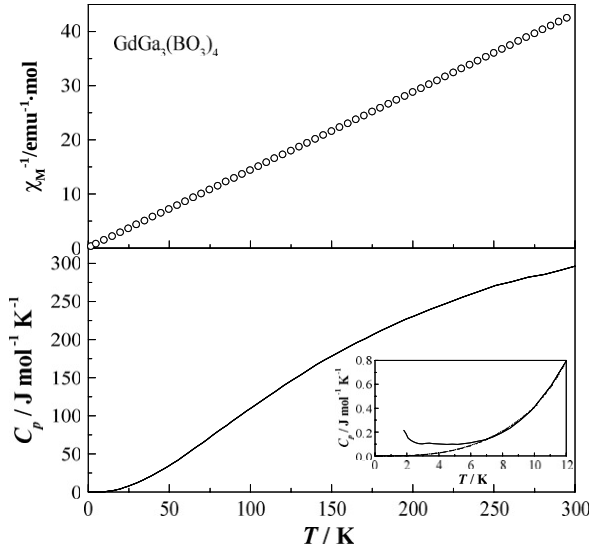

Fig. 12. Temperature dependence of the reciprocal magnetic susceptibility and the specific heat for $GdGa_3(BO_3)_4$. The inset shows the detailed temperature dependence of the specific heat below 12 K.

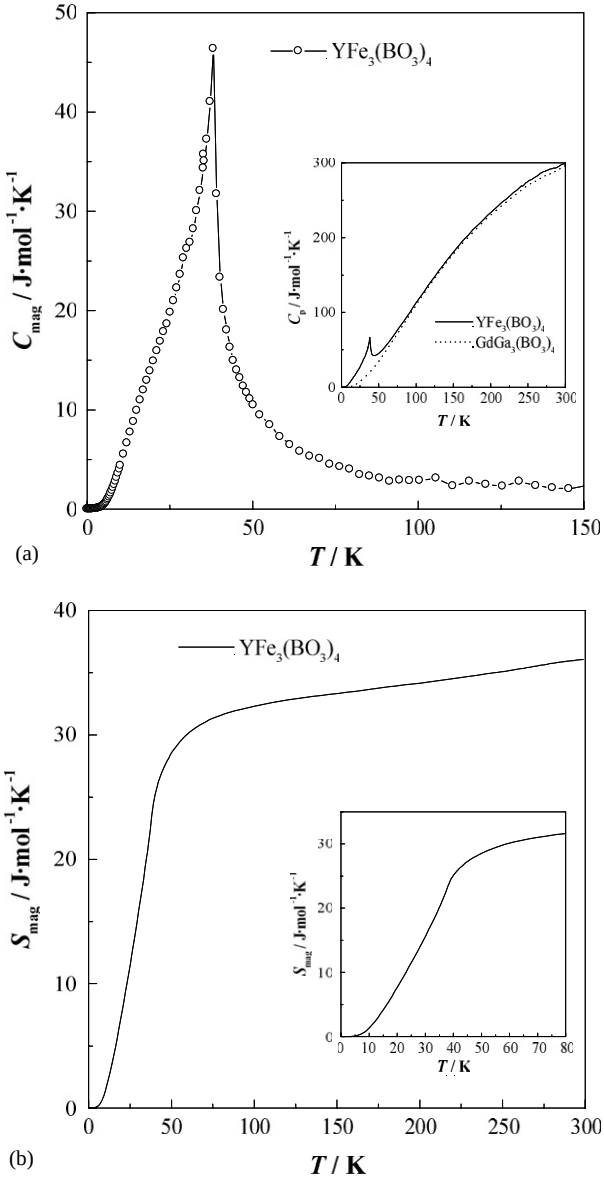

Fig. 13. (a) Temperature dependence of the magnetic specific heat (C_{mag}) for $YFe_3(BO_3)_4$. The inset shows the temperature dependence of the specific heat for $YFe_3(BO_3)_4$ and $GdGa_3(BO_3)_4$. (b) Temperature dependence of the magnetic entropy (S_{mag}) for $YFe_3(BO_3)_4$. The inset shows the detailed magnetic entropy in the temperature range below 80 K.

of $YFe_3(BO_3)_4$. The temperature dependence of the magnetic specific heat (C_{mag}) and the magnetic entropy change (S_{mag}) is shown in Figs. 13(a) and (b). The magnetic entropy change associated with this antiferromagnetic transition is obtained to be $\sim 30\,J\,mol^{-1}\,K^{-1}$ (at 60 K) by integrating $S_{mag}(T) = \int (C_{mag}/T)\,dT$. As will be described in the next section, the results of our ^{57}Fe Mössbauer measurements on the $EuFe_3(BO_3)_4$ (the isomer shift and the internal magnetic field of the Fe^{3+} ion) show that the Fe^{3+} ion is in the high spin state. The Fe^{3+} ion is considered to be in the high spin state for any of these $LnFe_3(BO_3)_4$ compounds, which has

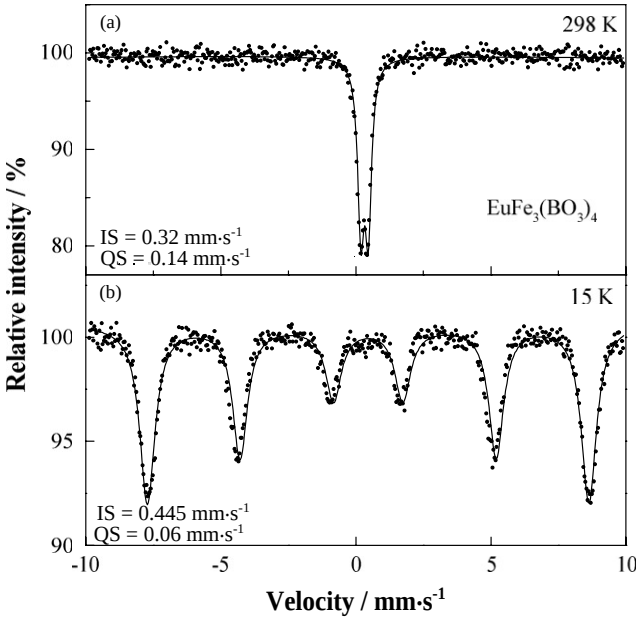

Fig. 14. Mössbauer spectra for $EuFe_3(BO_3)_4$ at 298 K (a) and 15 K (b). Solid lines correspond to fitting.

been also supported by the estimation of the effective magnetic moments for these compounds. So, the magnetic entropy change due to the arrangement of the Fe^{3+} ion in the $YFe_3(BO_3)_4$ is calculated to be $3R\ln(2S+1)=3R\ln(2\times 5/2+1)=3R\ln 6=44.7\,J\,mol^{-1}\,K^{-1}$, where R is the molar gas constant. Our experimental value $\sim 30\,J\,mol^{-1}\,K^{-1}$ is smaller than the estimated magnetic entropy change, but much larger than the magnetic entropy change calculated for the Fe^{3+} ion in the low spin state, i.e., $3R\ln(2S+1)=3R\ln(2\times 1/2+1)=3R\ln 2=17.3\,J\,mol^{-1}\,K^{-1}$. Experimental results that the magnetic entropy change determined by the specific heat measurements is lower than the estimated value may be ascribed to the beginning of magnetic transition at higher temperature. In fact, the magnetic entropy is still increasing above the magnetic transition temperature, 38 K (see Fig. 13(b)).

3.5. Mössbauer spectra

In order to obtain more information about the electronic state of Fe^{3+} ion in the antiferromagnetic state in these borates, we selected the $EuFe_3(BO_3)_4$ and have measured its Mössbauer spectra at above and below the magnetic transition temperature. Figs. 14(a) and (b) show the spectra measured at 298 and 15 K, respectively. The quadrupole splitting appears in the spectrum measured at 298 K. The spectrum at 15 K shows the magnetic hyperfine structure. Both the spectra indicate that all the Fe ions in the $EuFe_3(BO_3)_4$ compound are magnetically equivalent. The isomer shifts for the Fe^{3+} ion are $0.32\,mm\,s^{-1}$ (at 298 K) and $0.445\,mm\,s^{-1}$ (at 15 K), which are reasonable for this charge state [15]. The difference in isomer shifts between the 298 and 15 K spectra is due to a second-order Doppler shift [15]. The internal magnetic field at the nucleus of the Fe ion is obtained to be 51 T from the fitting of the experimental Mössbauer spectrum at 15 K. This value is reasonable for the internal magnetic field at the nucleus of the Fe^{3+} moments in the high spin state [16].

4. Summary

Rare-earth iron borates $LnFe_3(BO_3)_4$ (Ln = Y, La ~ Nd, Sm ~ Ho) show an antiferromagnetic transition at 22–40 K. It is due to magnetic interactions between Fe^{3+} ions. In addition, X-ray diffraction, specific heat, and DTA measurements indicate that a phase transition occurs for Ln = Eu ~ Ho, and Y compounds, and its transition temperature increases with decreasing the Ln^{3+} ionic radius from 88 K for $EuFe_3(BO_3)_4$ to 445 K for $YFe_3(BO_3)_4$.

References

[1] G. Blasse, A. Bril, Phys. Stat. Sol. 20 (1967) 551.
[2] V.I. Chani, M.I. Timoschechkin, K. Inoue, K. Shimamura, T. Fukuda, Inorg. Mater. 30 (1992) 1466.
[3] H.G. Danielmeyer, in: H.J. Queisser (Ed.), Festkörperprobleme XV, Pergamon Vieweg, Braunschweig, 1975.
[4] Y. Doi, Y. Hinatsu, J. Phys.: Condens. Matter 11 (1999) 4813.
[5] D. Harada, M. Wakeshima, Y. Hinatsu, J. Solid State Chem. 145 (1999) 356.
[6] M. Wakeshima, D. Harada, Y. Hinatsu, J. Mater. Chem. 10 (2000) 419.
[7] Y. Doi, Y. Hinatsu, K. Oikawa, Y. Shimojo, Y. Morii, J. Mater. Chem. 10 (2000) 797.
[8] Y. Izumiyama, Y. Doi, M. Wakeshima, Y. Hinatsu, K. Oikawa, Y. Shimojo, Y. Morii, J. Mater. Chem. 10 (2000) 2364.
[9] Y. Izumiyama, Y. Doi, M. Wakeshima, Y. Hinatsu, K. Oikawa, Y. Shimojo, Y. Morii, J. Phys.: Condens. Matter 13 (2001) 1303.
[10] Y. Sasaki, Y. Doi, Y. Hinatsu, J. Mater. Chem. 12 (2002) 2361.
[11] J.A. Campa, C. Cascales, E. Gutierrez-Puebla, M.A. Monge, I. Rasines, C. Ruiz-Valero, Chem. Mater. 9 (1997) 237.
[12] D.L. Graf, W.F. Bradly, Acta Crystallogr. 15 (1962) 238.
[13] N.I. Leonyuk, L.I. Leonyuk, Prog. Crystal Growth Charact. 31 (1996) 179.
[14] Y. Hashimoto, M. Wakeshima, K. Matsuhira, Y. Hinatsu, Y. Ishii, Chem. Mater. 14 (2002) 3245.
[15] Y. Hinatsu, K. Tezuka, M. Inamura, N.M. Masaki, Morii, J. Solid State Chem. 146 (1999) 253.
[16] E. Murad, J.H. Johnston, in: G.J. Long (Ed.), Mössbauer Spectroscopy Applied to Inorganic Chemistry, Vol. 2, Plenum Press, New York, 1984, pp. 507–582.